Role of Bi and Ga additives in the physical properties and structure of GeSe4-GeTe4 glasses

J. Szlęzak¹, J. Kelly², A. Ingram³,

Ya. Shpotyuk^{1,4}, S. Adamiak¹, A. Dziedzic¹, J. Cebulski¹, R. Golovchak^{2*}

¹Faculty of Mathematics and Natural Sciences, University of Rzeszow, Rzeszow, 35-959, Poland ²Department of Physics, Engineering and Astronomy, Austin Peav State University, Clarksville, TN

37044, USA

³Faculty of Physics, Opole University of Technology, Opole, 45370, Poland

⁴Department of sensor and semiconductor electronics, Ivan Franko National University of Lviv,

Lviv. 79000. Ukraine

Abstract

The influence of Bi on a structure and physical properties of mixed Ga-containing Ge-Se and Ge-Te

glasses is studied. Partially ordered nanoscale regions observed with high-resolution transmission

electron microscopy are compared with first sharp diffraction peak parameters determined through

neutron and X-ray scattering studies. Nanoindentation measurements show quite small deviations in

nanohardness (H) and Young's modulus (E) values for glasses with 1 and 5 at. % of Bi, while two

regions with different mechanical properties are observed for sample with 10 at. % of Bi. Increase in Bi

concentration from 1 at. % to 5 at.% leads to a complete opacity of ~2 mm thick glass in a whole IR

range of spectrum, while no drastic difference between these two samples is observed by SEM, TEM,

XRD and neutron scattering methods. Short-range order features and possible electron defect structure

are evaluated using EXAFS/XANES and PAL spectroscopies, respectively.

Keywords: nanostructured glasses; chalcogenides; nanoindentation; spectroscopy; electron

microscopy

* Corresponding author: Department of Physics, Engineering and Astronomy, Austin Peay State University, Clarksville, 601 College St., TN 37044, USA

E-mail address: holovchakr@apsu.edu (R. Golovchak). Tel.: +1 931 221-6361

1

1. Introduction

Chalcogenide glasses (ChG) are considered as convenient and cost-effective media for various applications in modern photonics, mostly because of their high IR transparency, excellent fiber drawing capability and large optical nonlinearities [1,2]. A number of Se and Te-based glasses and thin films have been proposed recently for applications in far-IR optics, optical waveguides, space telecommunication, sensor technologies, phase-change memory devices, etc. [1-6]. The ChG compositions are consistently being improved in order to optimize the efficiency and functionality of the devices [2,4-6]. As a rule, such refinement is achieved by changing the ratio between constituent chemicals or by mixing with new chemical elements. This approach, however, is almost exhausted for the binary and ternary ChG compositions, where most of the physical properties are studied across the entire glass-forming regions [2,7]. Using more than three constituents in ChG composition opens a wide range of possibilities for improving the medium properties, but simultaneously complicates enormously the understanding of its structure. This, in turn, limits our ability to develop adequate microstructural models that allow to predict the material's properties and reliability during exploitation in various conditions, and, as a consequence, to avoid undesirable effects.

Alternative approach to improve the initial properties of ChG relies on the nanoscale design, which also allows combination of two or more useful properties (mechanical, electronic, optical, magnetic, etc.) in one functional medium. In this regard, several chemical elements like Bi and Ga are found to modify ChG at the nanoscale by changing their type of conductivity, triggering local crystallization of amorphous matrix or creating partially ordered nanoscale inclusions [8-11]. In particular, giant infrared and visible light attenuation effect was discovered recently in Bi and Ga-containing Ge-Se-Te glasses, which mechanism is still not quite understood [12,13].

In this work, the physical properties of Bi and Ga-modified GeSe₄-GeTe₄ glasses are studied with total X-ray and neutron scattering (NS), Bragg high-energy X-ray diffraction (XRD), nanoindentation, scanning and transmission electron microscopies (SEM and TEM), positron annihilation lifetime (PAL) spectroscopy, extended X-ray absorption fine structure (EXAFS) and X-ray absorption near-edge

structure (XANES) methods. The observed nanoinhomogeneities can serve as a source of useful glass matrix modifications for various applications in optoelectronics and photonics.

2. Experimental

The ChG of $Bi_xGa_5(Ge_{0.2}Se_{0.8})_{50-(x+5)/2}(Ge_{0.2}Te_{0.8})_{50-(x+5)/2}$ system (Table 1) with x = 1 (Bi1), 5 (Bi5) and 10 (Bi10) were prepared by conventional melt quenching method using high-purity elements (5N or better). The appropriate amount of precursors with total mass ~25 g were vacuum sealed in silica ampoules of 10 mm in diameter. They were heated up to 900°C with 2°C/min heating rate, homogenized at this temperature for 12 hours in rocking furnace and quenched from 700°C into water at room temperature. To relieve the mechanical strains appeared as a result of rapid quenching, the specimens were additionally annealed at 160°C for 3h. All as-prepared samples were vitreous in nature, except the $Bi_{10}Ga_5Ge_{17}Se_{34}Te_{34}$ composition, which showed some crystalline reflexes in XRD patterns [14]. The compositions and purity of as-prepared materials were verified with X-ray photoelectron spectroscopy, showing no significant deviations from the nominal compositions or noticeable concentration of impurity complexes (oxygen-containing, in the first hand).

Optical transmission was measured with Bruker Vertex 70 spectrometer, using 2 mm thick ChG discs polished to a high optical quality with 1µm corundum powder in the final step.

The density, ρ , measurements were performed using Archimedes displacement method and Mettler Toledo analytical balances. Data were collected for bulk samples in ethanol at controlled room temperature and atmospheric pressure.

The CSM Instruments nanoindenter equipped with Berkovich-type pyramidal diamond tip (with radius of about 100 nm) was used to determine the values of nanohardness and reduced elastic modulus (the Young's modulus *E*). Before the measurements, nanoindenter was calibrated using standard sample of fused silica with elastic modulus of 73 GPa and Poisson's ratio of 0.17. Such calibration allowed reliable load and displacement resolution at the level of 10 nN and 0.1 nm, respectively. The load-displacement curves were recorded simultaneously, using 20 mN/min loading-unloading rate and 15 s dwell time at maximum load of 10 mN. Data analysis was performed using Oliver-Pharr method [15].

The surface of tested samples (polished before the measurements) was scanned in five randomly selected locations. At least five nanoindentation measurements where performed at each location. Such experimental measuring protocol allows a quite acceptable locality of each measuring test, eliminating the influence of indentation-size effects. The values of nanohardness, H, and Young's modulus E were statistically averaged. All nanoindentor fingerprints were observed by optical microscope and additionally characterized by atomic force microscope (AFM) in non-contact mode, both integrated with CSM UNHT system.

SEM equipped with energy-dispersive spectroscopy (EDS) analyzer FEI QUANTA 3D 200i was used for surface morphology studies and composition check. TEM (FEI Tecnai Osiris device) was used to investigate partially ordered phases in Bi1 and Bi5 samples at fine nanoscale.

The NS experiments were performed at Nanoscale-Ordered Materials Diffractometer (NOMAD) at Spallation Neutron Source, Oak Ridge National Laboratory. The bulk samples were measured in 3 mm quartz capillaries in an argon atmosphere to reduce scattering from the air. Three independent measurements for each sample's composition were performed to confirm the reproducibility of the results. The total X-ray scattering and Bragg XRD experiments were performed at the beamline 11-ID-B, Advanced Photon Source, Argonne National Laboratory, using synchrotron X-rays with wavelength 0.2127 Å and position sensitive Perkin Elmer amorphous silicon image plate detector [16]. These measurements were carried out at room temperature using coarse powdered (with mortar and pestle) samples sealed in Polyimide capillaries. The NS data were normalized with respect to the scattering from solid Vanadium rod, and the X-ray scattering data were corrected for background scattering, X-ray transmission and Compton scattering using PDFgetX2 software package developed by Qiu et al. [17]. Standard corrections for the area detector setup were applied [16]. After correction, the structure factor S(Q), which contains information on the atomic pair correlations in the investigated material, was extracted as described elsewhere [18].

EXAFS and XANES measurements were performed on powdered samples (glued onto a Kapton® tape) at X18B X-ray beamline at National Synchrotron Light Source, Brookhaven National Laboratory. EXAFS and XANES data were collected simultaneously at Ga *K*-edge (10.367 keV) and Bi

 L_3 -edge (13.419 keV) in a transmission mode, using sealed ion chambers of Oxford Danfysik filled with appropriate mixture of Ar/N₂ gases. The energy range was calibrated in respect to Se K-edge (12.658 keV) position by measuring pure Se as standard. Athena-Artemis software package [19] was used to process the experimental XANES/EXAFS spectra and extract the number of neighbors, N, the average nearest neighbor distance, R, and the Debye-Waller factor, σ_0^2 , for Ga atoms. Kaiser-Bessel type of window function was applied for restricting the EXAFS data in k space. The quick first shell theory incorporated into Artemis software was used as input for FEFF calculations [19]. Fit to the experimental EXAFS data was performed in R-space using Levenberg-Marquardt method of nonlinear least-squares minimization in Artemis [19].

PAL spectra were recorded using fast coincidence system (ORTEC) of 230 ps resolution (fwhm of a single Gaussian, determined by measuring ⁶⁰Co isotope) at the temperature of 18 °C and relative humidity of 45 %. Each PAL spectrum was measured with a channel width of 6.15 ps (total number of channels 8000) and contained 10⁶ coincidences in total. Isotope ²²Na (activity ~50 kBq) was used as the source of positrons (prepared from aqueous solution of ²²NaCl, wrapped with Kapton® foil of 7 μm thickness and sealed), which was sandwiched between two identical samples. All the PAL spectra of the investigated samples were approximated by a sum of discrete exponentials:

$$s(t) = \sum (I_i / \tau_i) \exp(-t / \tau_i),$$

with τ_i and I_i representing the positron lifetime and intensity of the i^{th} positron decay component. The standard LT 9.0 program [20] was used to fit the experimental curves. The uncertainties in the determination of lifetimes (τ_i) and corresponding intensities (I_i) are ± 0.005 ns and ± 0.5 %, respectively.

3. Results and discussion

The absence of strong crystalline reflexes in XRD patterns of Bi1 and Bi5 samples (Fig. 1) testifies their overall glassy nature, while the readable XRD reflexes in Bi10 sample (10 at.% of Bi) show the formation of Ga_2Se_3 and extended $Bi_2Se_nTe_{3-n}$ (n = 0, 0.5, 1, 1.5, 2) mixed crystallites. The latter were identified according to PDF database [21] and confirmed by SEM-EDS analysis, showing increased

concentration of Te and Bi chemical elements across the observed crystalline inclusions in Bi10 sample (Fig. 2b). The Ga₂Se₃ and crystallites of Bi₂Se_nTe_{3-n} solid solutions are not the only species, which can be formed in the multinary matrix of the investigated materials. At least five different phases crystallize during heating of Bi_xGa₅(Ge_{0.2}Se_{0.8})_{50-(x+5)/2}(Ge_{0.2}Te_{0.8})_{50-(x+5)/2} materials, as studied earlier [14]. In a low-temperature domain (~210-300 °C), which is just above the glass transition region, the crystallization of Te, Bi₂Se_nTe_{3-n} (n = 0, 0.5, 1, 1.5, 2) and Ga₂Se₂Te phases were identified with XRD. At higher temperatures (~320-370 °C), the crystallization of GeSeTe, GaGeTe and GeBi₂Te₄ phases occurred. Activation energy for crystallization in low-temperature domain increases with Bi concentration, while the overall crystallization starts at lower temperatures, indicating lower thermal stability of glasses with higher Bi content [14].

Besides the increased devitrification ability, the addition of Bi into Ga-containing (GeSe₄)-(GeTe₄) glasses leads to a general increase in their density (Table 1). The nanohardness, H, and Young's modulus, E, obtained through nanoindentation measurements (Fig. 3) follow the same trend while going from Bil to Bi5 sample, e.g. both these parameters show slight increase with Bi content: H increases from 3.02 GPa in Bi1 to 3.25 GPa in Bi5, E increases from 28.73 GPa in Bi1 to 30.43 GPa in Bi5 (Table 1). The deviations in H and E values for Bi1 and Bi5 were quite small (less than 0.5%) for different tested locations, which confirms good macroscopic homogeneity of Bi1 and Bi5 glasses and also absence of macroscopic voids (like bubbles, etc.) or significant density fluctuations. Results of nanoindentation measurements for Bi10 sample are more scattered, being considerably different for two observed regions arbitrary named as "bright area" and "dark area" (Fig. 3c). The average nanohardness $H = 3.17 \pm 0.15$ GPa obtained from the imprints in the "dark area" (imprints 4, 5 and 6 in Fig. 3c), correlates well with the values for Bi1 and Bi5 samples. Therefore, "dark area" can be identified as remaining amorphous matrix of Bi10 sample. Such matrix has a significant elastic component of the deformation, which can be ascertained form AFM image: depth of the indentation imprint for the "dark region" is ~215 nm (Fig. 4), while nanoindentor was intruded into the sample for ~500 nm. The average value of nanohardness $H = 2.26 \pm 0.10$ GPa obtained for the imprints in the "bright area" (imprints 1, 2 and 3 in Fig. 3c) is lower than for the host vitreous matrix and Ga_2Se_3 crystals ($H = 3.6 \pm 0.7$ GPa) [22], but higher

than for Bi₂Te₃ ($H = 1.6\pm0.2$ GPa) [23] and Bi₂Se₃ ($H = 0.9\pm0.1$ GPa) [24] single crystals. Therefore, the origin of "bright area" can be guessed as the regions with smashed by polishing Ga₂Se₃ and Bi₂Se_nTe_{3-n} crystallites, similar to those visible on a fresh fracture of Bi10 sample in Fig. 2.

Optical transmittance window for Bi1 sample extends from \sim 3 µm to \sim 16 µm (Fig. 5a) without any signature of significant impurities. It is typical transmission for purified amorphous chalcogenide semiconductors of that kind [2,6]. On the other hand, the Bi5 and Bi10 samples do not transmit electromagnetic radiation within this range (transmission is less than 1 % for \sim 2 mm thick Bi5 sample, see Fig. 5b). The non-transparency of Bi10 sample can be well explained by prevailing scattering of the light on crystalline inclusions of \sim 500 nm size and larger (Fig. 2), while the giant attenuation effect observed in Bi5 sample [12] cannot be attributed solely to this mechanism. The reason is that only partially-ordered regions of about \sim 5 nm dimensions (like quantum dots) can be observed with TEM in Bi5 sample, which is not enough to cause a significant Mie or Rayleigh scattering for IR light [25,26]. Moreover, similar partially-ordered \sim 5 nm-sized regions (though more rarely distributed) and even more extended \sim 100 nm Ga₂Se₃ seeds have been identified in Bi1 sample using TEM scanning elemental analysis (Fig. 6). The existence of Ga₂Se₃ seeds in Bi1 sample can also explain slight crystalline-like reflexes on top of the overall amorphous synchrotron XRD pattern (see insert to Fig. 1). The above inclusions, however, do not cause the opacity of Bi1 sample (Fig. 5a), while Bi5 sample, which on the other hand does not contain the larger \sim 100 nm seeds, is completely opaque (Fig. 5b).

If not the crystalline and partially-ordered inclusions, then the vitreous matrix itself should be examined towards the possible reason of giant light attenuation in Bi5 sample. Since the glassy state is characterized by the absence of long-range ordering in the atomic arrangements, the medium- and short-range orders are to be investigated. The information on the medium-range order can be obtained by analysing the first sharp diffraction peak (FSDP) [27-29], observed at around $\sim 1 \text{ Å}^{-1}$ in S(Q) structure factor of Bi1 and Bi5 glasses determined from both synchrotron X-ray and neutron scattering data (Table 2, Fig. 7). If we assume that FSDP in glass originates from some kind of periodicity in real space, like crystalline Bragg peaks but at the medium range order scale [28], it is possible to estimate size of such regions using Scherrer-like equation $L\cong 2\pi/\Delta Q$ [Å], where ΔQ is full width at half maximum (fwhm) of

FSDP peak. The estimated dimensions of such regions from the fwhm of FSDP measured for Bi1 and Bi5 samples are within the range of 2.4-2.5 nm (Table 2). They are lower than the average size of partially-ordered regions (\sim 5 nm in diameter) observed with TEM (Fig. 8), which interlayer distance \sim 0.314 nm (determined from electron diffraction pattern) roughly corresponds to d (h k l) = d (0 l 5) of Bi₂Se_{1.5}Te_{1.5} crystal [21,30,31]. Although FSDP has more complicated origin than just the size of partially-ordered fragments and cannot be described explicitly by only one structural parameter (concentration of cations, degree of density fluctuations, order/disorder ratio, etc.), the similarity of FSDP parameters for Bi1 and Bi5 samples suggests that there is no significant structural difference between these two vitreous matrices at the medium range order scale. So, if the opacity of Bi5 sample is caused by atomic arrangement, the short-range order has to be further examined.

EXAFS and XANES techniques are used in this paper to elucidate the peculiarities of short-range ordering in the investigated materials. Because the giant light attenuation effect is observed in Bi5 glass, which main difference from Bi1 sample is the higher Bi to Ga ratio in the composition and higher number of quantum dot-like regions, we have focused on the behaviour of these two chemical elements in Ge-Te-Se matrix. Therefore, Ga K-edge EXAFS (Fig. 9a) and Bi L₃-edge XANES spectra (Fig. 9b) have been investigated and analysed. The fitting of Ga K-edge EXAFS spectra (Fig. 10, Table 3) shows that Ga atoms prefer 4-fold coordination in all the investigated materials and the nearest neighbour distance is typical for Ga-Se distances in Ga-Ge-Se glasses (the data for Ga_{6.8}Ge_{17.9}Se_{75.3} glass is shown for comparison [10]). It means that Ga prefers to be connected with Se atoms, which correlates well with the data of TEM scanning elemental analysis across ~100 nm size crystallites (Fig. 6) – ultimate result of such preferential bonding. Similarity of EXAFS spectra (Fig. 9a) and their fitting parameters (Table 3) for Bi1, Bi5 and Bi10 samples allows to conclude that Ga-based structural arrangements are rather not responsible for the giant attenuation effect in Bi5 sample.

Contrary to Ga, the Bi L₃-edge XANES spectra (also known to be sensitive to the ionic state of the absorber [32,33]) show a considerable shape difference for Bi1 and Bi5 glasses, compare to Bi10 or Bi₂Se₃ samples (Fig. 9b) where Bi is known to form crystallites. In the latter case Bi should be in Bi³⁺ state, which is also consistent with corresponding shape of L₃-edge XANES spectrum [33]. The huge

change within ~150 eV distance from Bi L₃ edge as observed for Bi5 sample (Fig. 9b), the most probably, is due to a significant contribution from multiple scattering around Bi atoms [34]. In contrast to single scattering, which prevails in the high-energy EXAFS region, multiple scattering depends strongly on the angles between scatterers and is thus very sensitive to local environment of the absorbing atom, but simultaneously is much more complicated for modelling. Whichever the case, the observed difference in L₃-edge XANES spectra of Bi1, Bi5 and Bi10 samples leads to a conclusion that Bi has a substantially different environment in Bi1, Bi10 and Bi5 samples, and, thus, could play a key role in understanding the giant attenuation effect observed in Bi5 sample [12]. It could have, for example, the coordination higher than three, forming polyhedral units similar to Bi-containing oxide glasses [35].

In order to evaluate possible defect structure associated with Bi dopants, PAL spectroscopy was applied, which is known to be especially sensitive to free-volume defects devoid of electron density at the sub/nanometer scale. The positron trapping rate in such defects essentially depends on their size and associated effective charge [36-38]. So, if Bi forms any kind of defects associated with electron density redistribution, it should be possible to characterize them through the changes in positrons lifetime [37,38]. Sensitivity of PAL method to small nanosize voids in ChG structure allows their quantification and characterization, which would help to eliminate from consideration the mechanism associated with light scattering on these voids, which are considered as the main reason of high light attenuation in ChG fibers [26]. Experimentally measured PAL spectra for Bi1, Bi5 and Bi10 materials are shown in Fig. 11. An acceptable goodness of fit was achieved with just two exponential components (τ_1 , I_1) and (τ_2 , I_2), excluding any positronium formation from consideration. This, in turn, leads to a conclusion that there is no significant fraction of nm-size free volume (voids) in Bi1, Bi5 and Bi10 materials. PAL data (Table 4) show significant decrease in the average lifetime of positrons for Bi10 sample, while difference between PAL data of Bi1 and Bi5 glasses is subtle, only slightly exceeding the associated uncertainties. Such behaviour correlates well with electric conductivity of these materials: Bi1 and Bi5 samples show typical behaviour for narrow-bandgap semiconductors, while Bi10 sample possesses electrical conductivity typical for conductors [12]. A subtle difference between PAL spectra of Bi1 and Bi5 samples suggests that Bi in Bi5 glass does not form any open-volume defects associated with effective

negative charge. So, the idea on Bi-based polyhedra with coordination of Bi higher than three looks plausible.

4. Conclusions

On the basis of the performed investigations it can be concluded that uniform nanostructured glasses of Bi_xGa₅(Geo_{.2}Seo_{.8})_{50-(x+5)/2}(Geo_{.2}Teo_{.8})_{50-(x+5)/2} family with x=1 at.% and x=5 at.% of Bi content (Bi1 and Bi5 compositions studied) can be obtained by conventional melt-quenching technique. Their nanohardness and Young's modulus both increase from 3.02 GPa and 28.73 GPa in Bi1 glass to 3.25 GPa and 30.43 GPa in Bi5 glass, respectively. Although no significant crystalline reflexes were found in Bi1 and Bi5 XRD patterns, the Ga₂Se₃ crystallites/seeds (~100 nm in diameter) and Bi₂Se_{1.5}Te_{1.5} (~5 nm in diameter) partially-ordered nanoscale inclusions have been identified with TEM. The medium range order, estimated through FSDP analysis of neutron and synchrotron X-ray scattering data, is found to be similar in both samples. Same conclusion can be drawn for the short-range order around Ga atoms, which are found to be 4-fold coordinated with Se atoms in all glasses. On the other hand, the local environment around Bi shows a significant difference for Bi1 and Bi5 compositions as determined from Bi L₃-edge XANES. This difference, however does not lead to a substantial electron density redistribution, as testified with PAL method. So, the mechanism of the observed giant light attenuation effect in Bi5 glass requires further thorough investigations, also involving electron excitation/decay experiments.

5. Acknowledgements

JS acknowledge support of this work provided by CampusFrance via BGF joint-PhD Cotutelle scholarship programme. Work performed at Argonne National Lab and use of the Advanced Photon Source were supported by the U. S. Department of Energy, Office of Science, Office of Basic Energy Sciences, under Contract No. DE-AC02-06CH11357. APSU team acknowledges Joerg C. Neuefeind, Katharine Page, Matthew Tucker and Jue Liu for help with neutron and X-ray scattering experiments.

RG acknowledges U.S. National Science Foundation (Grant No. DMR-1725188) for the acquisition of PAL spectrometer.

References

- [1] B.J. Eggleton, B. Luther-Davies, K. Richardson, Chalcogenide photonics, Nature Photon. 5 (2011) 141–148.
- [2] J-L. Adam and X. Zhang (Eds), Chalcogenide Glasses: Preparation, properties and application, Woodhead Publishing series in Electronic and Optical Materials No.44, 2014.
- [3] D. Lencer, M. Salinga, M. Wuttig, Design rules for phase-change materials in data storage applications, Adv. Mater. 23 (2011) 2030–2058.
- [4] P. Lucas, Z. Yang, M.K. Fah, T. Luo, S. Jiang, C. Boussard-Pledel, M-L. Anne, B. Bureau, Telluride glasses for far infrared photonic applications, Opt. Mater. Express 3 (2013) 1049.
- [5] S. Cui, C. Boussard-Plédel, J. Troles, B. Bureau, Telluride glass single mode fiber for mid and far infrared filtering, Opt. Mater. Express 6 (2016) 971-978.
- [6] S. Cui, R. Chahal, Ya. Shpotyuk, C. Boussard, J. Lucas, F. Charpentier, H. Tariel, O. Loreal, V. Nazabal, O. Sire, V. Monbet, Z. Yang, P. Lucas, B. Bureau, Selenide and telluride glasses for mid-infrared bio-sensing, Proc. SPIE 8938 (2014) 893805-1-9.
- [7] G. Yang, Y. Gueguen, J-C. Sangleboeuf, T. Rouxel, C. Boussard-Plédel, J. Troles, P. Lucas, B. Bureau, Physical properties of the Ge_xSe_{1-x} glasses in the 0 < x < 0.42 range in correlation with their structure, J. Non-Cryst. Solids 377 (2013) 54–59.
- [8] Y. Liu, Sh. Yuan, J. Xie, F. Shangguan, J. Ren, G. Chen, A Study on crystallization kinetics of thermoelectric Bi₂Se₃ crystals in Ge–Se–Bi chalcogenide glasses by differential scanning calorimeter, J. Am. Ceram. Soc. 96 (2013) 2141–2146.
- [9] T-Y. Lee, C. Kim, Y. Kang, D-S. Suh, K.H.P. Kim, Y. Khang, Rapid crystallization of GeTe–Bi₂Te₃ mixed layer, Appl. Phys. Lett. 92 (2008) 101908-1-3.
- [10] R. Golovchak, L. Calvez, E. Petracovschi, B.Bureau, D.Savytskii, H.Jain, Incorporation of Ga into the structure of Ge–Se glasses, Mater. Chem. Phys. 138 (2013) 909–916.
- [11] R. Golovchak, Ya. Shpotyuk, V. Nazabal, C. Boussard-Pledel, B. Bureau, J. Cebulski, H. Jain, Study of Ga incorporation in glassy arsenic selenides by high-resolution XPS and EXAFS, J. Chem. Phys. 142 (2015) 184501-1-10.

- [12] R. Golovchak, Ya. Shpotyuk, J. Szlęzak, A. Dziedzic, A. Ingram, J. Cebulski, Giant VIS-IR light attenuation effect in nanostructured narrow-bandgap glasses, Opt. Lett. 43 (2018) 387-390.
- [13] R. Golovchak, A. Kozdras, T. Hodge, J. Szlęzak, C. Boussard-Pledel, Ya. Shpotyuk, B. Bureau, Optical and thermal properties of Sb/Bi-modified mixed Ge-Ga-Se-Te glasses, J. Alloys Compd. 750 (2018) 721-728.
- [14] L. Saturday, C. Johnson, A. Thai, J. Szlęzak, Ya. Shpotyuk, R. Golovchak, Devitrification of Biand Ga-containing germanium-based chalcogenide glasses, J. Alloys Compd. 674 (2016) 207-217.
- [15] W.C. Oliver, G.M. Pharr, Measurement of hardness and elastic modulus by instrumented indentation: Advances in understanding and refinements to methodology, J. Mater. Res. 19 (2004) 3-20.
- [16] P.J. Chupas, X. Qiu, J.C. Hanson, P.L. Lee, C.P. Grey, S.J.L. Billinge, Rapid-acquisition pair distribution function (RA-PDF) analysis, J. Appl. Crystallogr. 36 (2003) 1342–1347.
- [17] X. Qiu, J.W. Thompson, S.J.L. Billinge, PDFgetX2: a GUI-driven program to obtain the pair distribution function from X-ray powder diffraction data, J. Appl. Crystallogr. 37 (2004) 678.
- [18] R. Golovchak, P. Lucas, J. Oelgoetz, A. Kovalskiy, J. York-Winegar, Ch. Saiyasombat, O. Shpotyuk, M. Feygenson, J. Neuefeind, H. Jain, Medium range order and structural relaxation in As-Se network glasses through FSDP analysis, Mater. Chem. Phys. 153 (2015) 432-442.
- [19] B. Ravel, M. Newville, *ATHENA, ARTEMIS, HEPHAESTUS*: data analysis for X-ray absorption spectroscopy using *IFEFFIT*, J. Synchrotron Radiat. 12 (2005) 537–541.
- [20] J. Kansy, Microcomputer program for analysis of positron annihilation lifetime spectra, Nucl. Instr. Meth. Phys. Res. A 74 (1996) 235-244.
- [21] S. Kabekkodu (Ed.), PDF-4+ 2015 (Database), International Centre for Diffraction Data, Newtown Square (PA), 2015.
- [22] Elena Petracovschi. Vitrocéramiques infrarouges pour application à la vision nocturne. Matériaux.

 Université Rennes 1, 2014. Français. <NNT : 2014REN1S058>. (https://tel.archivesouvertes.fr/tel-01127397)

- [23] C. Lamuta, A. Cupolillo, A. Politano, Z.S. Aliev, M.B. Babanly, E.V. Chulkov, M. Alfano, L. Pagnotta, Nanoindentation of single-crystal Bi₂Te₃ topological insulators grown with the Bridgman-Stockbarger method. Phys. Stat. Solidi 253 (2016) 1082–1086.
- [24] Sh. Gupta, N. Vijayan, A. Krishna, K. Thukral, K. K. Maurya, S. Muthiah, A. Dhar, B. Singhe, G. Bhagavannarayana, Enhancement of thermoelectric figure of merit in Bi₂Se₃ crystals through a necking process, J. Appl. Cryst. 48 (2015) 533–541.
- [25] C.E. Barnett, Some applications of wave-length turbidimetry the infrared, Wave-length Turbidimetry in the Infrared (1941) 69-75.
- [26] J. S. Sanghera, L. E. Busse, and I. D. Aggatwal, Effect of scattering centers on the optical loss of As& glass fibers in the infrared, J. Appl. Phys. 75 (10) (1994) 4885-4891.
- [27] S.R. Elliott, Origin of the first sharp diffraction peak in the structure factor of covalent glasses, Phys. Rev. Lett. 67 (1991) 711-714.
- [28] A.C. Wright, Longer range order in single component network glasses?, Phys. Chem. Glasses: Eur. J. Glass Sci. Technol. B 49 (2008) 103-117.
- [29] G. N. Greaves, S. Sen, Inorganic glasses, glass-forming liquids and amorphizing solids, Adv. Phys. 56 (2007) 1-166.
- [30] E. Požega, S. Ivanov, Z. Stević, L Karanović, R. Tomanec, L. Gomidželović, A. Kostov, Identification and characterization of single crystal Bi₂Te_{3-x}Se_x alloy, Trans. Nonferrous Met. Soc. China 25 (2015) 3279–3285.
- [31] J. R. Wiese, L. Muldawer, Lattice constants of Bi-Te and Bi-Se solid solution alloys, J. Phys. Chem. Solids 15 (1960) 13-16.
- [32] D.C. Koningsberger, R. Prins (Eds.), X-Ray Absorption: Principles, Applications, Techniques of EXAFS, SEXAFS and XANES, John Wiley & Sons, New York, 1988.
- [33] N. Jiang, J.C.H. Spence, Can near-edge structure of the Bi L3 edge determine the formal valence states of Bi?, J. Phys.: Condens. Matter 18 (2006) 8029–8036.
- [34] J.J. Behr, Recent developments in Multiple-Scattering Calculations of XAFS and XANES, DOE/ER/45416-6.

- [35] Y.G. Choi, K.H. Kim, V.A. Chernov, J. Heo, EXAFS spectroscopic study of PbO-Bi₂O₃-Ga₂O₃ glasses, J. Non-Cryst. Solids 259 (1999) 205-211.
- [36] R. Krause-Rehberg, H. Leipner, Positron annihilation in Semiconductors, Springer, Heidelberg, 1999.
- [37] O. Shpotyuk, J. Filipecki, Free volume in vitreous chalcogenide semiconductors: Possibilities of positron annihilation lifetime study, WWSzP, Czestochowa, 2003.
- [38] Ya. Shpotyuk, S. Adamiak, A. Dziedzic, J. Szlezak, W. Bochnowski, J. Cebulski, Nanoscale inhomogeneities mapping in Ga-modified arsenic selenide glasses, Nanoscale Res. Letters 12 (2017) 88-1-5.

Table 1. Density, molar volume, nanohardness H and Young's modulus E of studied materials.

Sample	Sample	Density, g/cm ³	Н,	Ε,
Sample	Sample	Density, g/cm	GPa	GPa
Bi1	Bi ₁ Ga ₅ Ge _{18.8} Se _{37.6} Te _{37.6}	5.083±0.005	3.02±0.02	28.73±0.14
Bi5	Bi ₅ Ga ₅ Ge ₁₈ Se ₃₆ Te ₃₆	5.345±0.005	3.25±0.02	30.43±0.01
Bi10	Bi ₁₀ Ga ₅ Ge ₁₇ Se ₃₄ Te ₃₄	5.624±0.005	3.17 ± 0.15	28.25 ± 0.84
			(dark area)	(dark area)
			2.26 ± 0.10	27.86 ± 1.03
			(bright area)	(bright area)

Table 2. FSDP and first peak (Peak 1) parameters determined from synchrotron X-ray and neutron scattering data per Gaussians' fit.

		FSDP			Peak 1			
	Sample	Q (Å-1)	fwhm (Å-1)	Area (a.u.)	L (nm)	$Q(Å^{-1})$	fwhm (Å-1)	Area (a.u.)
NS	Bi1	1.028	0.247	0.057	2.54	2.048	0.409	0.518
	Bi5	1.023	0.252	0.052	2.49	2.051	0.408	0.441
	Bi10*	1.023	n/a	n/a	n/a			
XRD	Bi1	1.071	0.257	0.035	2.44	2.026	0.415	0.543
	Bi5	1.051	0.262	0.037	2.40	2.032	0.425	0.605
	Bi10*	1.048	n/a	n/a	n/a			

^{* -} partially crystallized (positions of first crystalline reflexes are shown)

Table 3. Fitting parameters and their statistical deviation for Ga K-edge Fourier transformed EXAFS spectra of Ga_{6.8}Ge_{17.9}Se_{75.3} [10], Bi1, Bi5 and Bi10 glasses: R – distance from neighboring atom to the absorbing atom; σ_0^2 – Debye-Waller factor; N – local coordination number.

K-edge		Ga	
	R (Å)	σ_{θ}^{2} (Å ²)	N
Composition	±0.02	± 0.001	±0.6
Ga6.8Ge17.9Se75.3	2.42	0.0077	4.2
Bi ₁ Ga ₅ Ge _{18.8} Se _{37.6} Te _{37.6}	2.41	0.0069	4.2
Bi ₅ Ga ₅ Ge ₁₈ Se ₃₆ Te ₃₆	2.42	0.0062	4.0
Bi ₁₀ Ga ₅ Ge ₁₇ Se ₃₄ Te ₃₄	2.42	0.0078	4.5

Table 4. Fitting parameters describing the two-component reconstructed PAL spectra in studied glasses.

Sample	τ_l (ns)	<i>I</i> ₁ (%)	τ ₂ (ns)	I ₂ (%)	τ_{av} (ns)
	±0.005	±0.5	±0.005	±0.5	± 0.002
Bi1	0.230	62.1	0.405	37.9	0.296
Bi5	0.226	61.8	0.401	38.2	0.293
Bi10	0.214	58.0	0.383	42.0	0.285

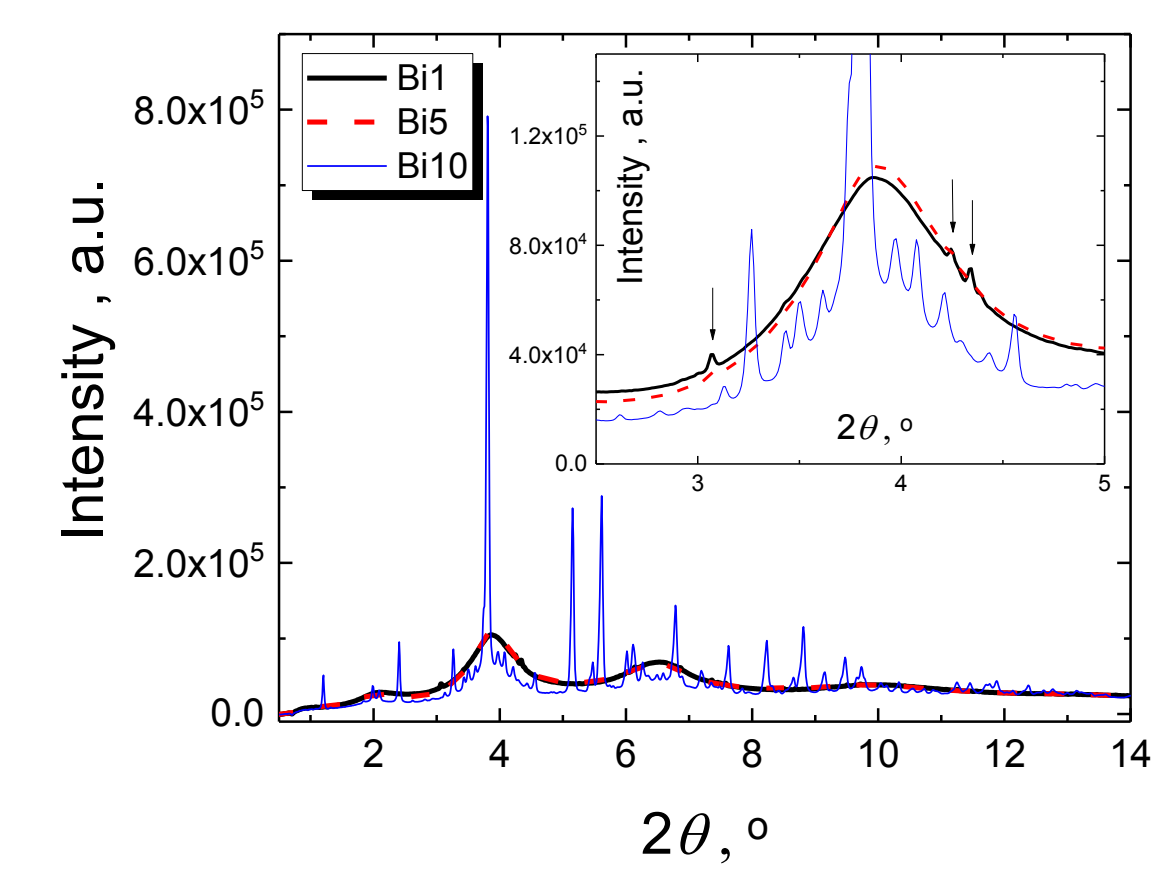


Fig. 1. Synchrotron XRD patterns of studied materials. The insert shows magnified fragment with readable reflexes of Ga₂Se₃ seeds (pointed by arrows) for Bi1 sample.

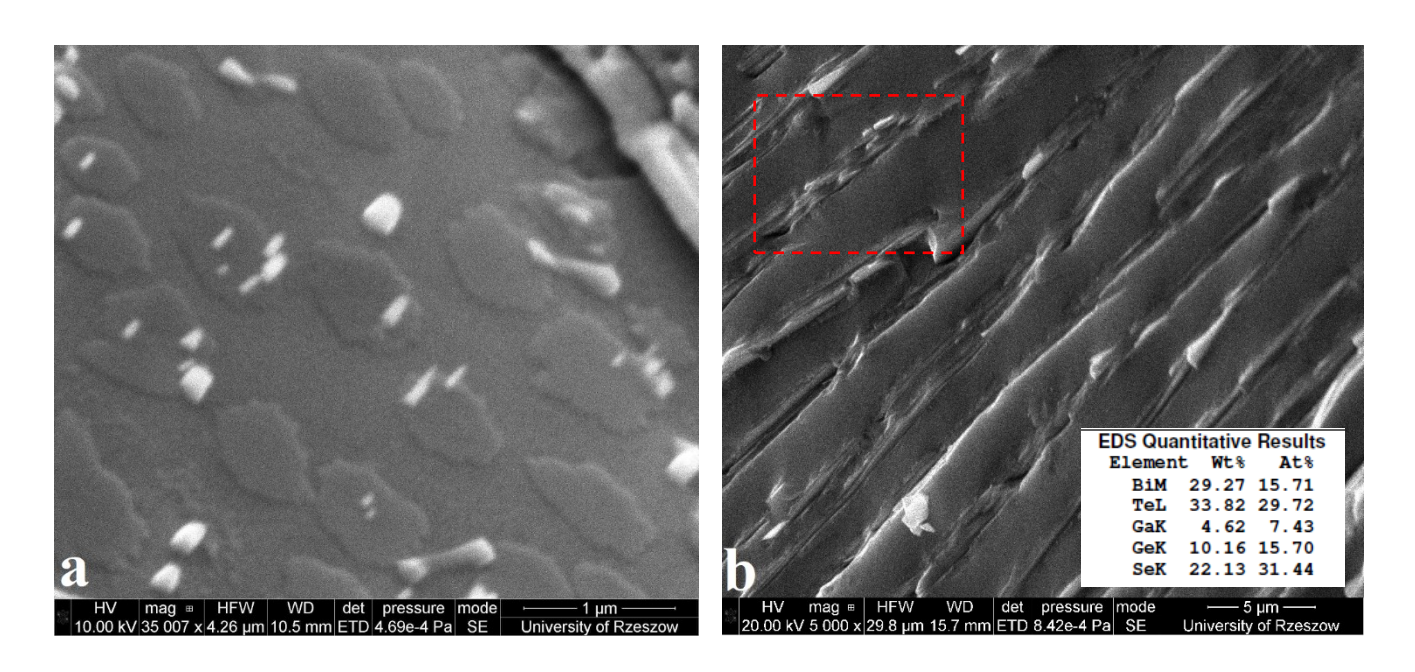


Fig. 2. SEM-EDS micrographs of fresh fracture of Bi10 sample. Figure (a) shows Ga₂Se₃ crystallites embedded into residual vitreous matrix. Figure (b) shows presumably Bi₂Se_nTe_{3-n} crystalline inclusions in the form of lamellae-like structure.

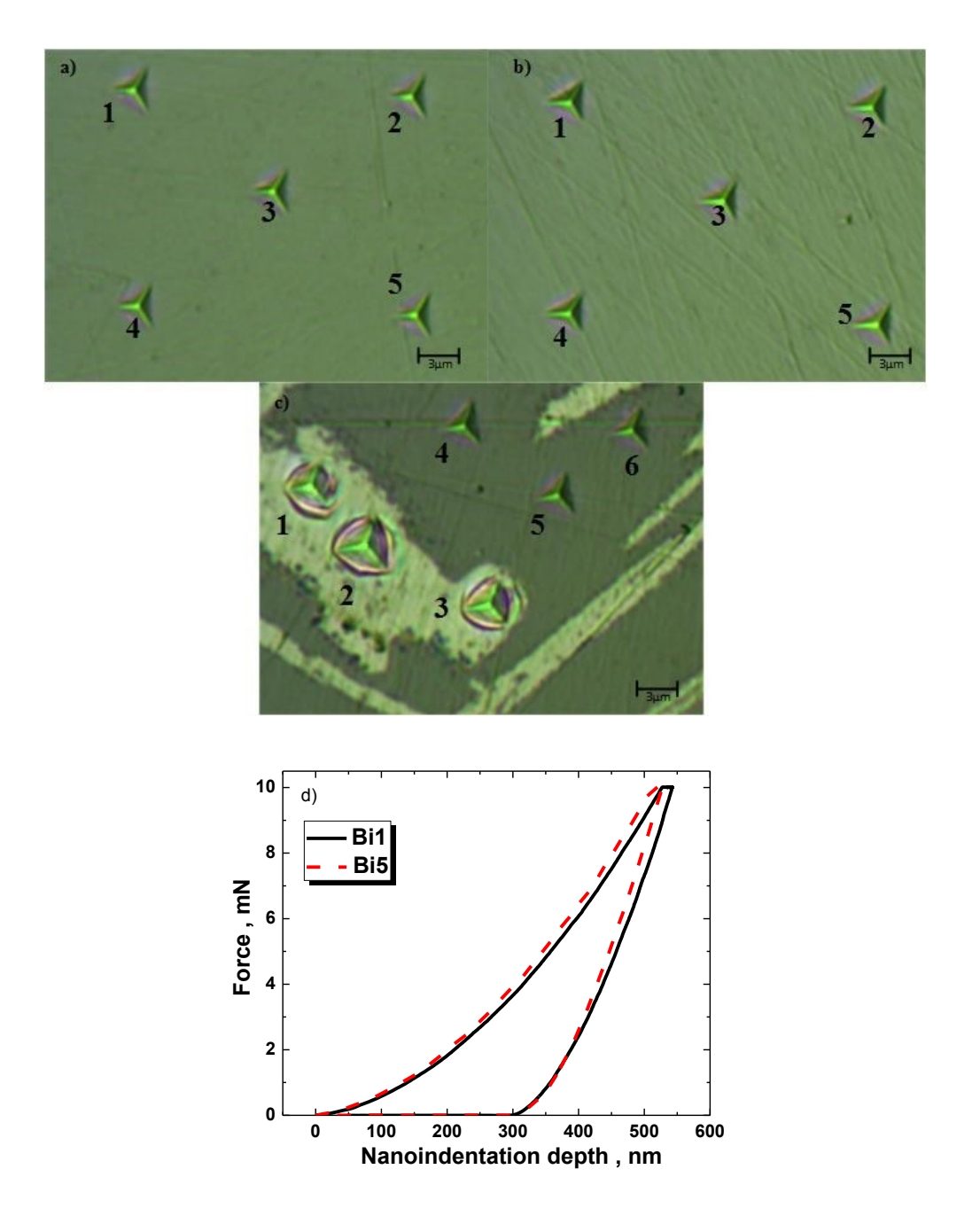


Fig. 3. Nanoindentor fingerprints and load-displacement curves. Figure (a) shows 5 fingerprints for Bi1 sample, figure (b) shows 5 fingerprints for Bi5 sample, and figure (c) shows 3 fingerprints in the "dark area" and 3 fingerprints in the "bright area" for Bi10 surface. Figure (d) shows nanoindentation load-displacement curves for Bi1 and Bi5 samples.

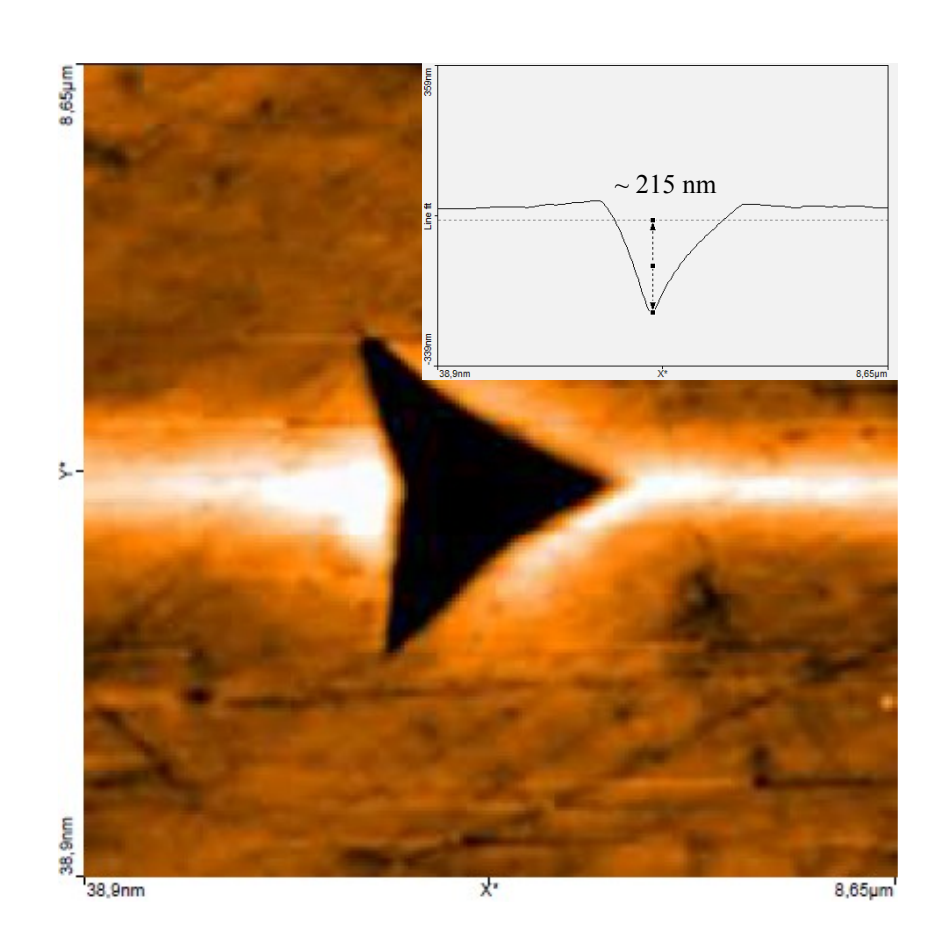


Fig. 4. AFM image of nanoindentation imprint for Bi10 sample (dark area). Depth profile is shown in the insert.

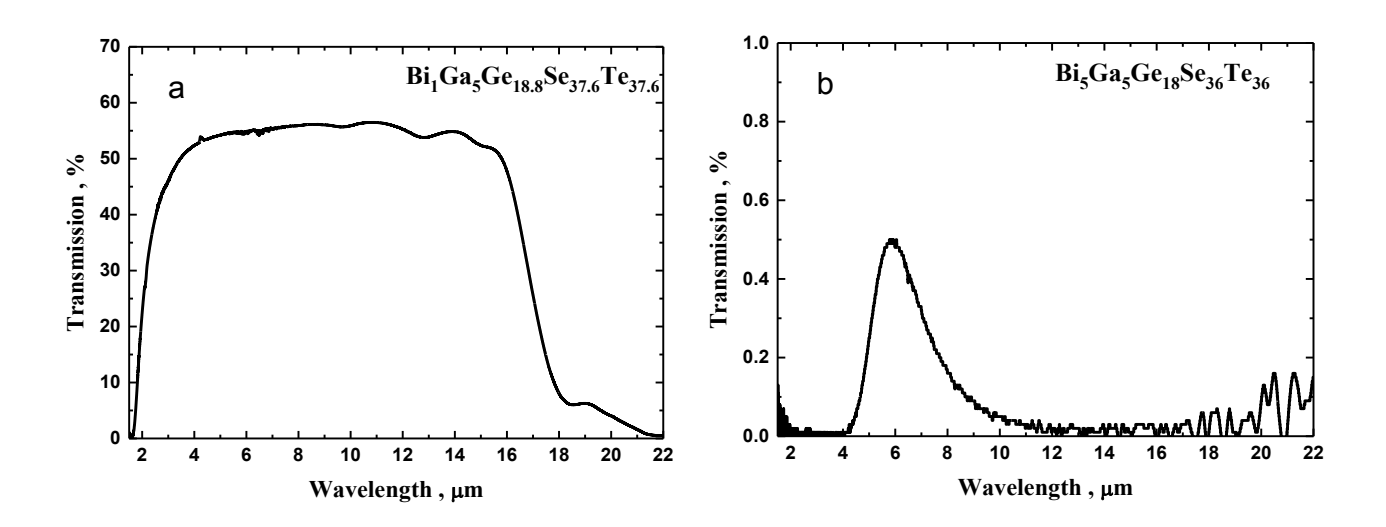


Fig. 5. Optical transmission spectra of Bi1 (a) and B5 (b) samples. It is clearly seen, that increase of Bi concentration to 5 at.% makes a \sim 2 mm thick sample completely opaque in 2-22 μ m range.

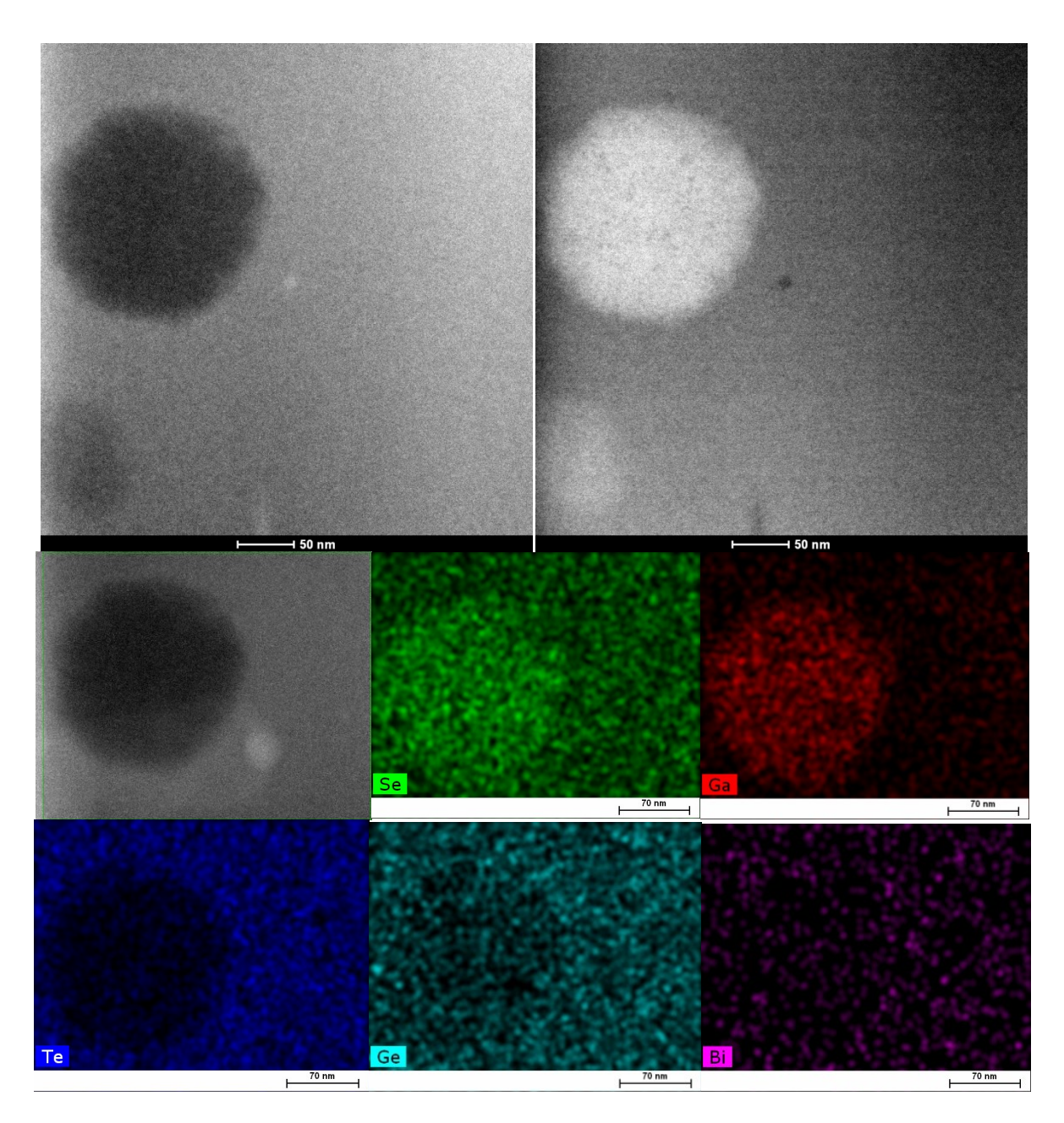
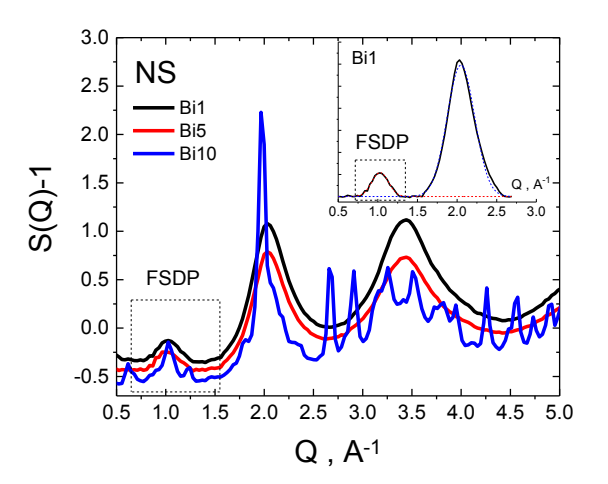


Fig. 6. Elemental scanning TEM images. Top-left picture shows STEM HAADF image, top-right picture shows STEM bright field image of \sim 100 nm crystalline inclusions found in Bi1 sample. The chemical composition mapping of Se, Ga, Te, Ge and Bi elements across such region (bottom panels) allows to identify these inclusions as Ga_2Se_3 seeds.



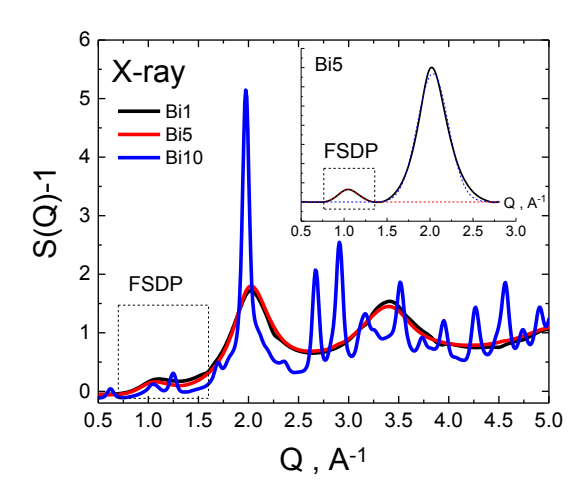


Fig. 7. Neutron scattering (NS) and X-ray scattering results. Structure factors S(Q) as obtained from NS and synchrotron X-ray scattering data for the investigated samples show overall vitreous nature of Bi1 and Bi5 samples and number of crystalline reflexes in Bi10 sample. Inserts show the region with FSDP and first structural peak after background subtraction, fitted with Gaussians.

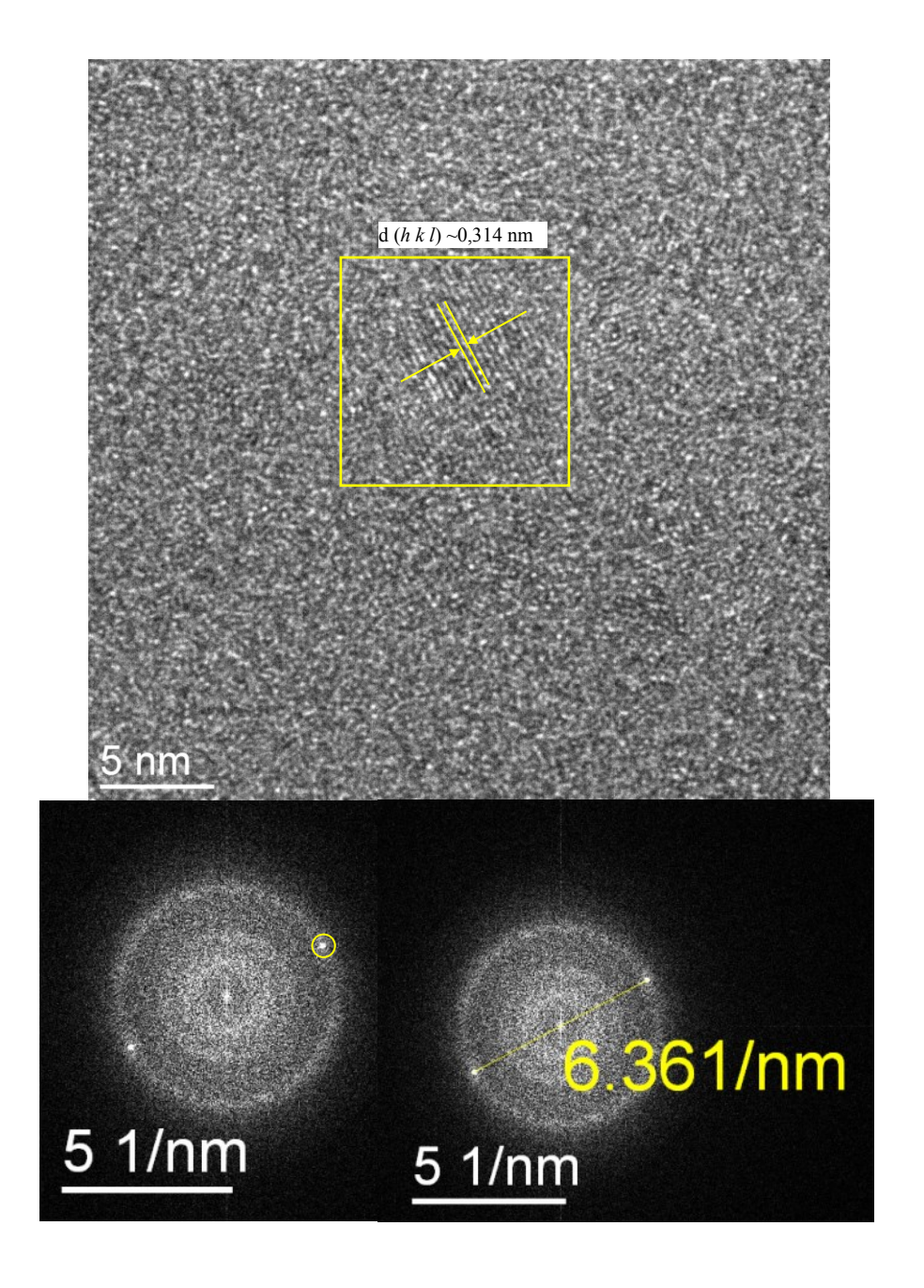
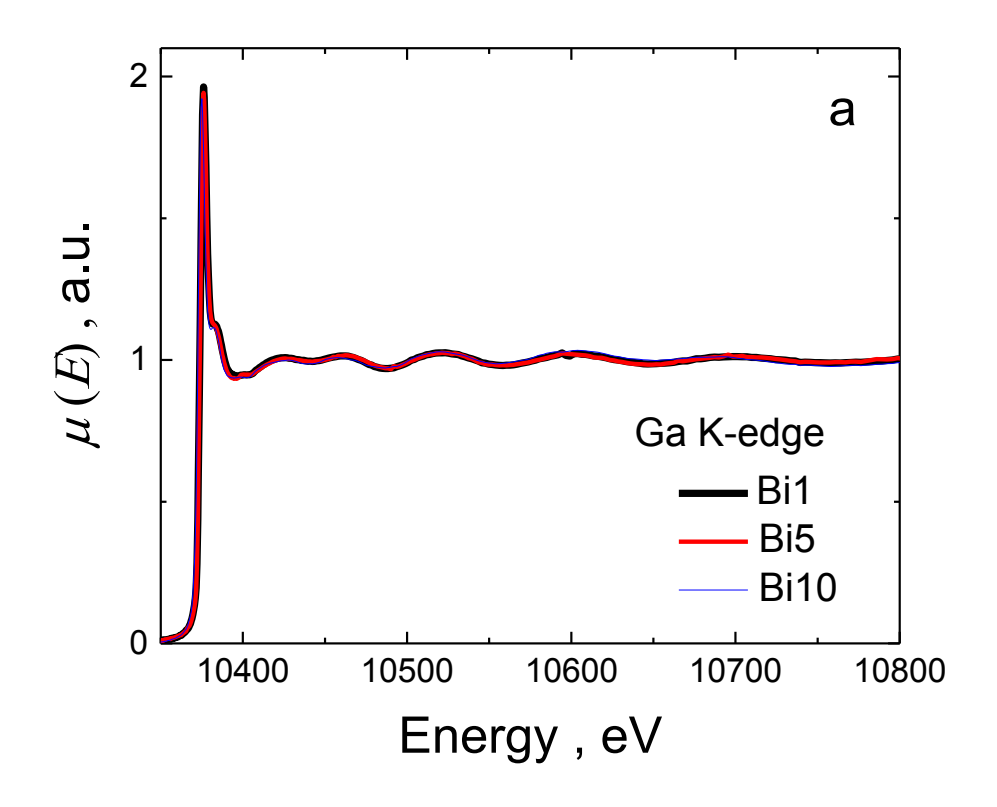


Fig. 8. High resolution TEM image of typical small partially-ordered region observed in Bi1 and Bi5 samples. The electron diffraction pattern gives interlayer distance ~ 0.314 nm, which roughly corresponds to d (h k l) = d (0 1 5) of Bi₂Se_{1.5}Te_{1.5} crystal [21,30,31].



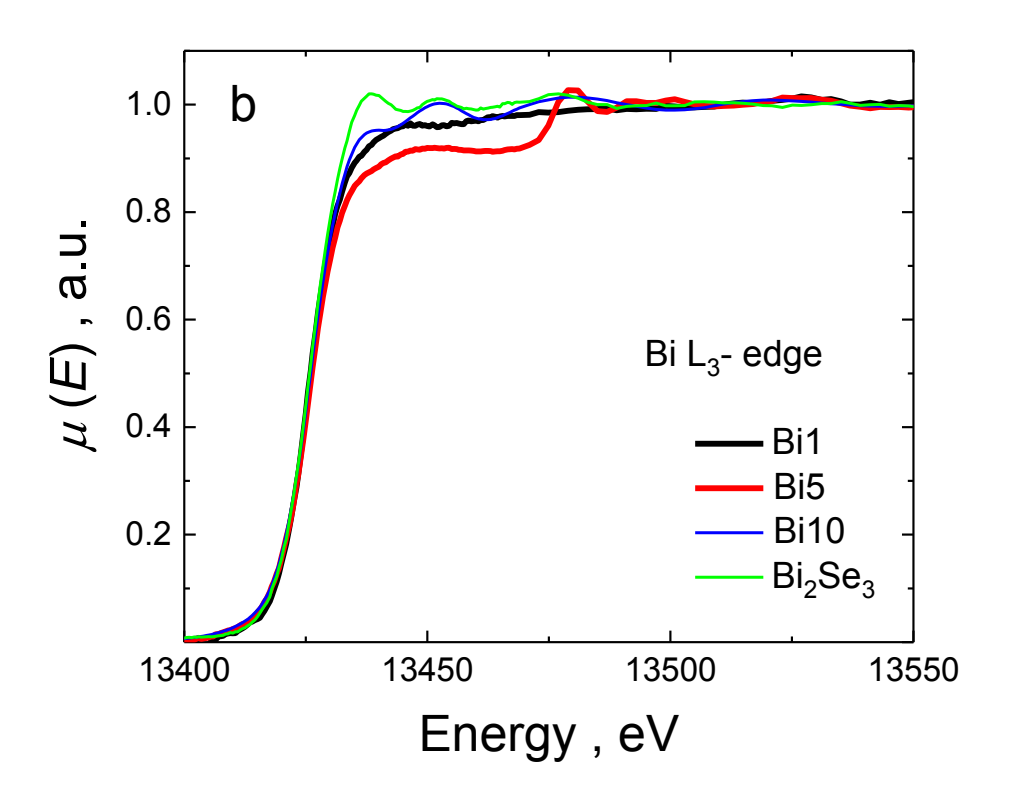


Fig. 9. EXAFS and XANES spectra collected at Ga K-edge (a) and Bi L₃-edge (b), respectively. A huge difference for Bi local environment in Bi5 and all the other samples is observed.

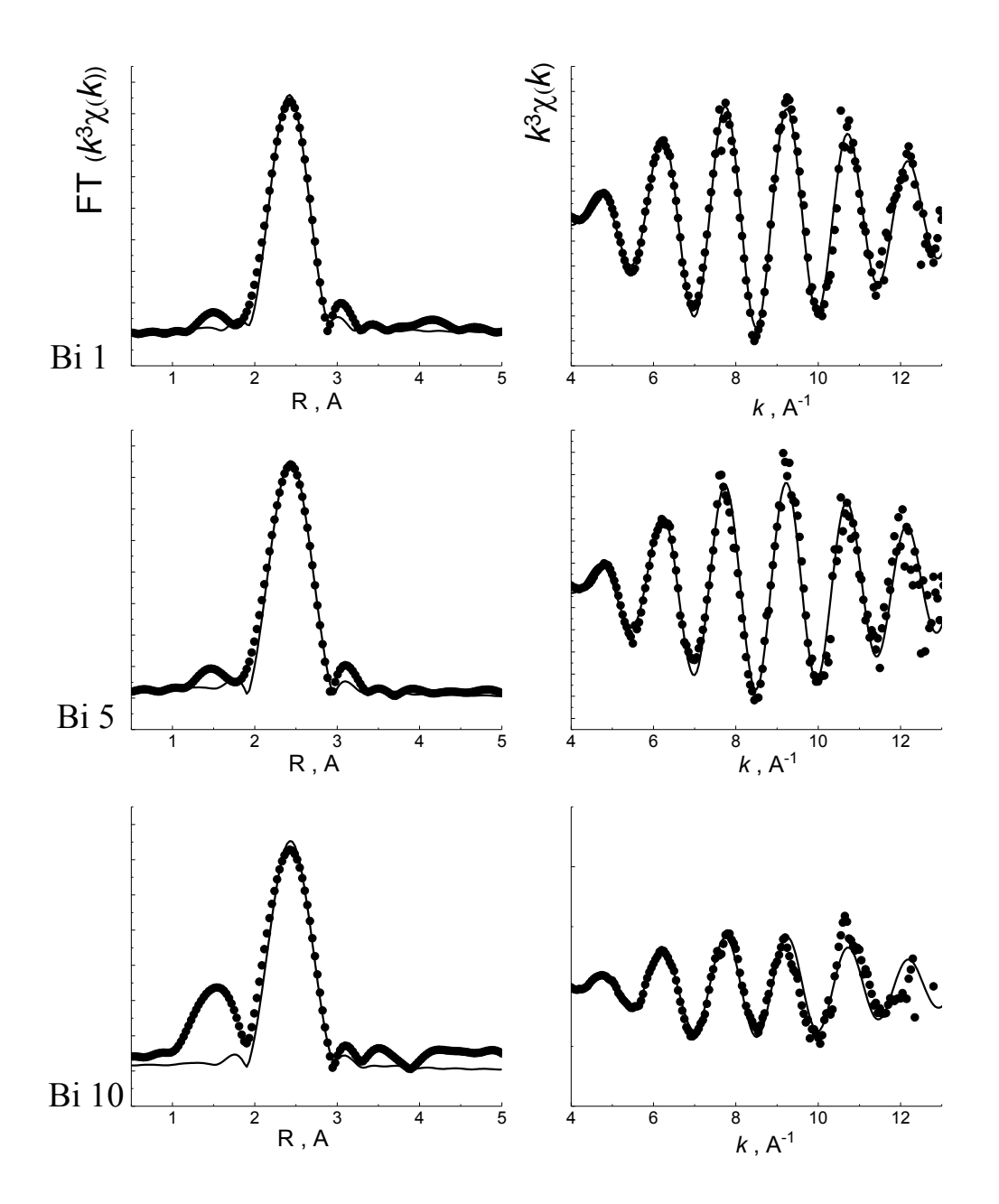


Fig. 10. The k^3 -weighted $\chi(k)$ EXAFS oscillations (right panel) at Ga K-edge and their Fourier Transform (left panel). Solid curves correspond to the quick first shell theory fit in Artemis software [19], used to determine the number of nearest neighbors around Ga atoms and corresponding interatomic distances.

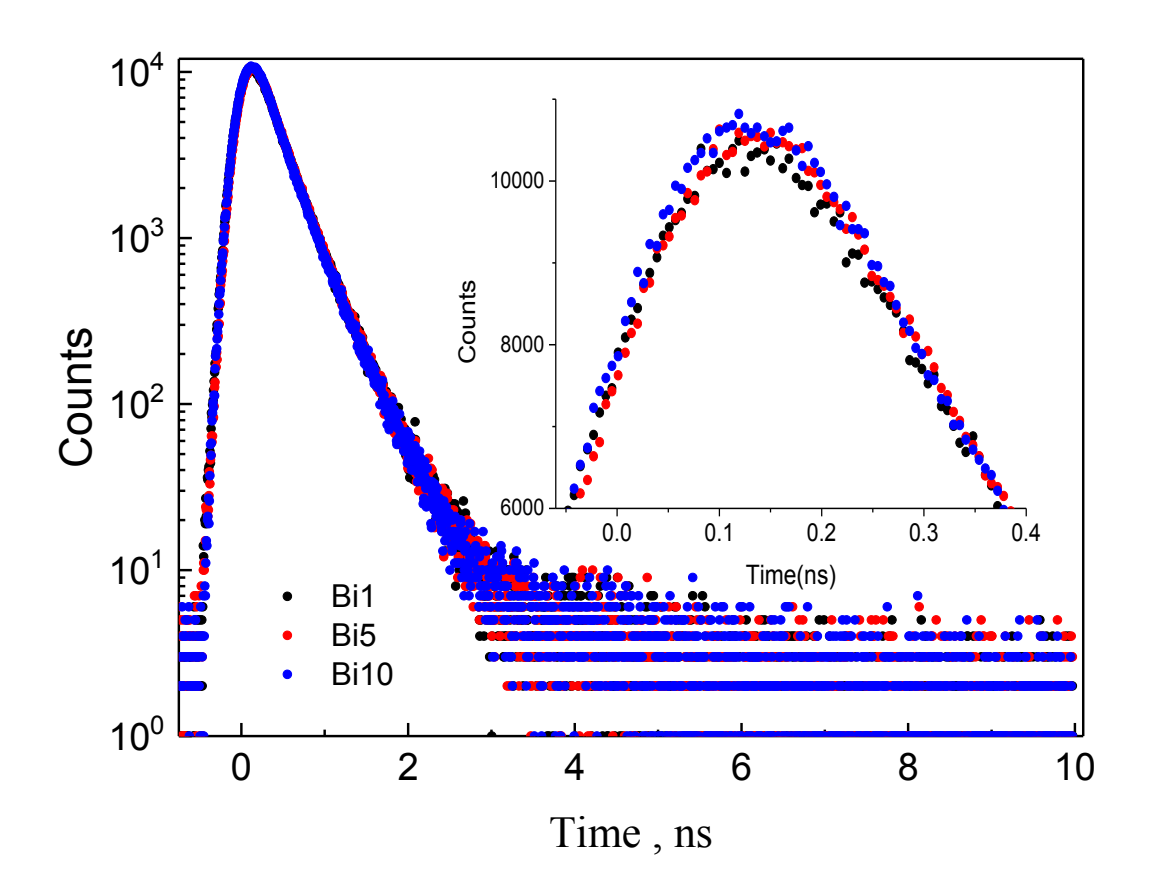


Fig. 11. Comparison of raw PAL spectra for Bi1, Bi5 and Bi10 samples. The insert shows a magnified peak region, which suggests only a subtle difference between Bi1 and Bi5 samples.